Research Article
https://doi.org/10.33904/ejfe.1430606

Eur J Forest Eng 2024, 10(1):54-66.

EJFE

Identification of the Leaves of *Ulmus pumila* L., *Tilia cordata* Mill. and *Acer campestre* L. Using Vegetation Indices

Pavel A. Dmitriev*, Boris L. Kozlovsky, Anastasiya A. Dmitrieva, Tatiana V. Varduni

Southern Federal University, Rostov-on-Don, Russia

Abstract

The aim of the research was to evaluate a group of vegetation indices (VIs) for identifying the leaves of some species including *Ulmus pumila* L., *Tilia cordata* Mill. and *Acer campestre* L. Hyperspectral imaging (HSI) was carried out under artificial lighting in laboratory conditions using a Cubert UHD-185 hyperspectral camera. A technique was developed for the automated selection of pure spectral profiles from hyperspectral images by setting a double barrier specified by intervals of PSSR and NDVI VIs. A total of 80 VIs was calculated. A statistical analysis of the data was carried out to determine their representativeness. The VIs that were most dependent on the species characteristics of the trees were determined using analysis of variance (ANOVA) and principal component analysis (PCA) methods. Research has shown that the PCA method is effective and sufficient to identify the group of VIs characterized by the highest dispersion related to tree species. The PCA carried out for pairs of tree species made it possible to identify a group of vegetation indices, the value of which to the greatest extent depends on species characteristics. These VIs are Carter2, CI2, CRI4, GMI2, mSR2, NDVI2, OSAVI2, SR1, Carter4, Datt2, SR6, Datt, DD, Maccioni, MTC.

Keywords: Hyperspectral imaging, Principal component analysis, Region of interest, Species classification, Woody plants.

1. Introduction

Natural and artificial forests, urban green spaces, and protective forest belts need regular monitoring to assess their resources, ecological state, and presence of invasive species. On a regional scale, this is possible only with the help of Unmanned Aerial Vehicles (UAV) and various remote sensing tools. The first problem to be solved is to identify the species. In some cases, for example, when identifying alien species invasions, it is important to have a method for identifying plants in real-time for their subsequent destruction. The problem of identifying species has been successfully solved for agricultural crops (Heupel et al., 2018; Saeed et al., 2021), which are represented over large areas by single species agrocenoses. Remote forest inventory and monitoring still have many limitations. The main limitation is the complexity of forest structure and composition (Fassnacht et al., 2024). According to a modern review of sources on this issue (Dainelli et al., 2021), tree identification and mapping using remote sensing data is an active area of research. Progress has been made in identifying tree species using spectral characteristics obtained from satellites and UAVs (Modzelewska et al., 2020; Sothe et al., 2020; Egli and Höpke, 2020; Grabska et al., 2020; Onishi and Ise, 2021; Hermosilla et al., 2022). Spectral characterization sensors include not only spectroradiometers and multispectral cameras but also hyperspectral cameras. (Cao et al., 2018; Dmitriev et al., 2022a; 2022b). Several studies have demonstrated that spectral characteristics alone are inadequate for accurately identifying forest species. Therefore, it is necessary to combine them with textural characteristics (Zhang et al., 2023; Zhong et al., 2022; Chen et al., 2023). Furthermore, there is an issue with the repeatability of spectral values over time (van der Werff et al., 2022). In general, the use of plant spectral characteristics as taxonomic traits requires evidence.

In the context of this problem, it is proposed to test the following hypothesis: in a laboratory experiment (with maximum control of external factors) for tree species that differ significantly in morphological and ecological characteristics from each other (for example; *Ulmus pumila*, *Tilia cordata,* and *Acer campestre*), it is possible to determine a group of vegetation indices (VIs) and the mathematical interpretation of the values that can be used for their species identification.

*Corresponding Author: Tel: + 7 9604500405 E-mail: pdmitriev@sfedu.ru
Received: 02 February 2024; Accepted: 26 April 2024

2. Materials and Methods

The research was conducted in the Botanical Garden of the Southern Federal University (SFedU Botanical Garden), Rostov-on-Don, Russia (Figure 1). Coordinates of the study area: 7°16′25.63″N; 39°19′13.59″E. The climate of Rostov-on-Don is temperate continental, and arid, with moderately mild winters and hot summers. The sum of active temperatures is 3200-3400 °C. The average annual air temperature is +9.2 °C. During the year, the average monthly air temperature ranges from −5 °C in January to +23.2 °C in July. The absolute minimum temperature is −31.9 °C, and the absolute maximum temperature is +40.1 °C. The average annual rainfall is 569 mm. The total precipitation for the frost-free period is 323 mm (Panov et al., 2006).

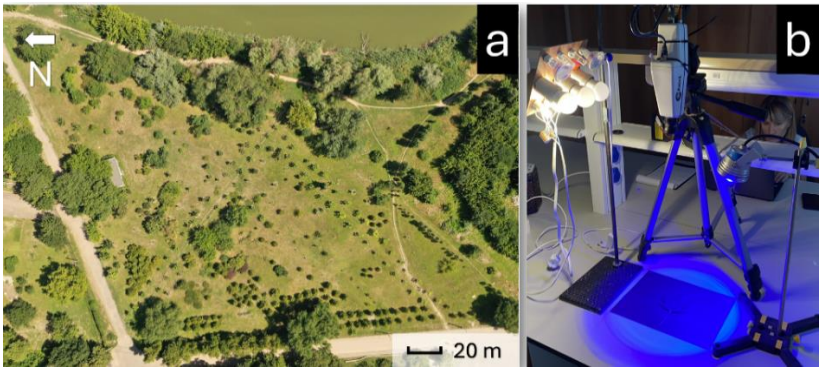

Figure 1. Research region (a) and measurement system (b).

The leaves of *Ulmus pumila* L., *Tilia cordata* Mill. and *Acer campestre* L. were identified as these are large trees widespread in the region and grow naturally and are widely used for landscaping settlements. All experimental plants are of similar age, at the same stage of ontogeny (young generative specimens), and grow under similar conditions in the park of the SFedU Botanical Garden, located in the floodplain of the Temernik River. Each of the three species was represented in the experiment by three samples. From each sample, five leaves were selected in a circle from their crown from the base of the shoot of the current year.

Hyperspectral imaging (HIS) was carried out under artificial lighting in laboratory conditions using a Cubert UHD-185 hyperspectral camera (Aasen et al., 2015; Bareth et al., 2015). Four halogen and one blue LED lamp were used to illuminate the object.

A leaf was placed on a black tracing paper. The camera lens was located 70 cm from the leaf blade and directed perpendicular to it. HSI of each leaf was carried out five times. The pixel size was about 35 mm^2. This survey technique gives a stable result, which can be demonstrated by the example of the change in the NDVI value in a series of five images of one leaf (Figure 2).

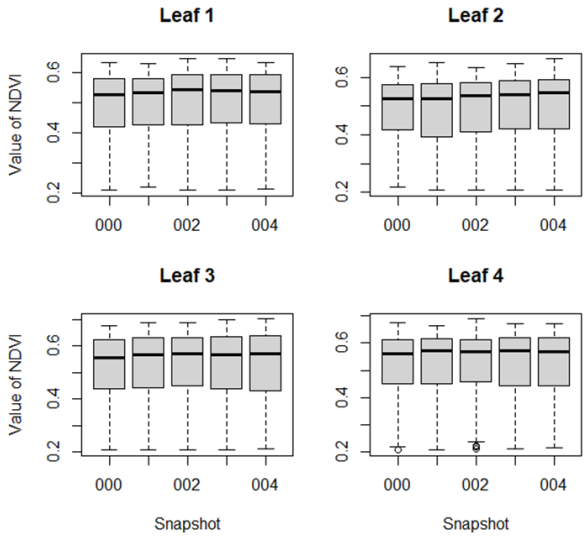

Figure 2. Boxplots of NDVI values in a series of four images of an *A. campestre* leaf, specimen 1 (HSI date: Aug 26).

Based on the HSI data, 80 VIs were calculated (supplementary Table 1). Visualization of VIs values with reference to spectral profiles in the HSI data was implemented in the R programming environment (R Core Team). This makes it possible to visualize the results of manipulations with spectral profiles in the image and to identify VIs that «do not read» the plant object (supplementary Table 2). Statistical and mathematical analysis was carried out in the R programming environment.

3. Results and Discussion

For analysis, the selection of the spectral profiles from HSI data by the operator is a problem. This process is not only labor-intensive and time-consuming but also subjective. This underscores the urgent need to develop an automated method for selecting «pure» spectra based on a unified approach. Our proposed technique involves selecting and processing all the spectral profiles, and then based on the value of the «green indices», choosing only those that corresponded to the green leaf. This principle, similar to determining crop yields using NDVI, excludes index values below 0.2 from the calculations (Vannoppen et al., 2020). The technique was tested on the data of spectral imaging of leaf blades of *U. pumila*, *T. cordata* and *A. campestre*, obtained in laboratory conditions (Figure 3).

The task was to separate the background and mixed spectra, simultaneously capturing the leaf and the background. The presence of mixed spectra in the sample set can lead to the accumulation of a systematic error in calculating of VI values because their number depends on the size and shape of the leaf blade. Thus, the proportion of mixed spectra increases from simple to lobed leaves and large to small leaves. NDVI was chosen as such an index. This index gives reliable results and is widely used. The operator selected «pure» spectra from the hyperspectral images and calculated the NDVI range corresponding to the green leaf. It amounted to an interval of 0.5 – 1.0. A preliminary analysis of histograms of the magnitude distribution of other «green» VIs from the sets of spectra that give NDVI values in the range of 0.5 – 1.0, showed that they are close to a normal distribution (Figure 4).

However, with this approach, the distribution of the NDVI itself becomes asymmetric (Figure 5). Therefore, it was decided to select «pure» spectra based on the ranges of two VIs. To search for the second VI, regressions of the values of other VIs from the NDVI value were constructed. As an illustration, the regression of VI values from the NDVI value of the leaves of *A. campestre,* sample № 1, survey date Aug 26, is shown (Figure 6, supplementary Table 3).

a b c

Figure 3. Hyperspectral images of leaves *A. campestre* (a), *U. pumila* (b) and *T. cordata* (c).

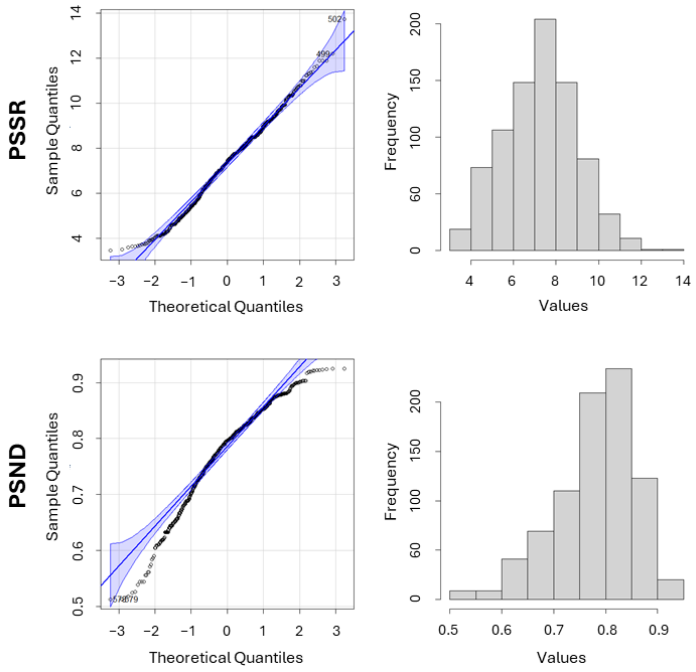

Figure 4. VIs PSSR and PSND distributions for leaves of *A. campestre* (Aug 26, sample № 1) by value, obtained from a set of spectra with an NDVI value in the range from 0.5 to 1.0.

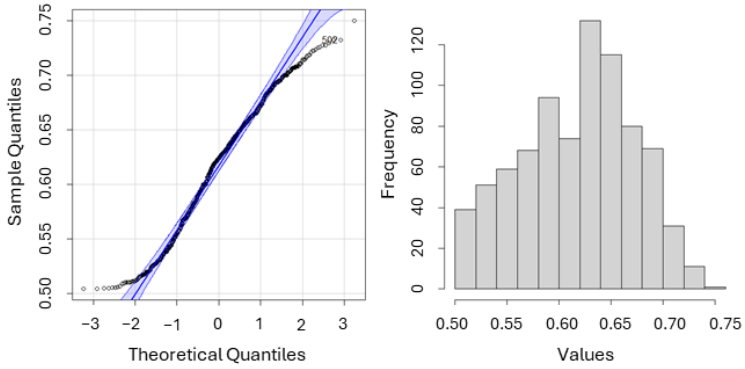

Figure 5. The distribution of NDVI in the range from 0.5 to 1.0 for the leaves of *A. campestre* (Aug 26, sample № 1).

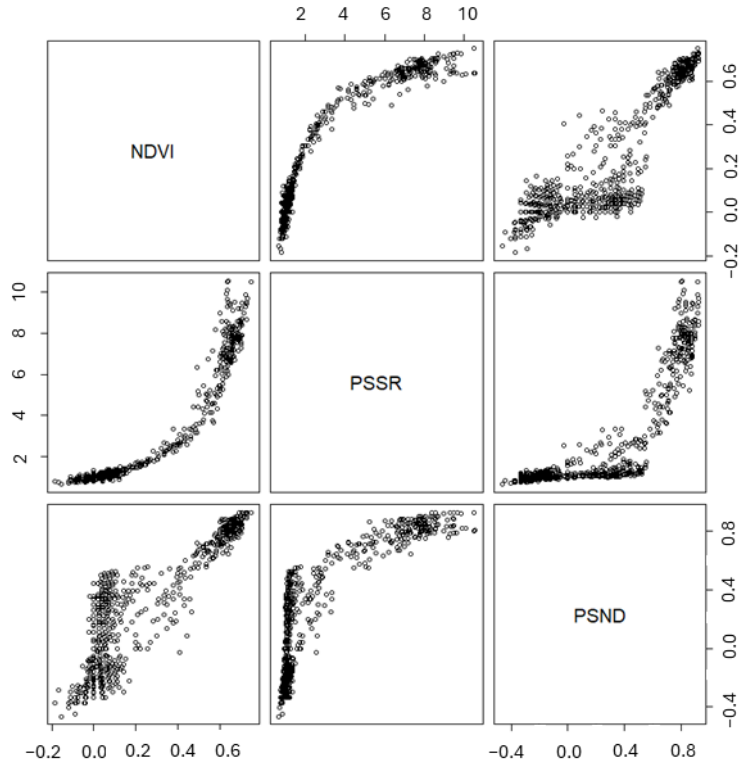

Figure 6. Regression of VIs PSSR and PSND values from NDVI value for leaves of *A. campestre* (Aug 26, sample № 1).

Of interest are indices for which the regressions of their values from the NDVI value are curvilinear, such as PSSR, MCARI2, MTVI, or are presented as two clearly delimited fields (background and leaf) such as PSND, CARI, CRI2 (supplementary Table 3). When calculating these VIs, combinations of spectral bands are used other than those used for NDVI, so the use of these indices in pairs can increase the reliability of selecting «pure» spectra. Indices that give linear regressions with NDVI with a close relationship close to functional are not suitable for solving the problem since the same channels are used in their calculation; for example, DWSI4, SAVI, PRI_norm, and SR. (supplementary Table 3).

PSSR was chosen as the second VI, which sets an additional boundary for forming a set of «pure» spectra (Figure 6). The range of values of this index, corresponding to a green leaf, lies from 5 to 10. It was calculated based on data received by the operator. Thus, for VI calculations, spectra were selected that give NDVI values of more than 0.5 with a PSSR value of more than 5. An exception was made for NDVI and PSSR – the NDVI value was calculated from a set of spectra that give PSSR values greater than 5, and the PSSR value was calculated from a set of spectra that give NDVI values greater than 0.5. The results of the selection of spectra by this technique can be demonstrated in Figure 7. In contrast to the known methods for selecting objects by SB, selecting a region of interest by a threshold of two VIs is simpler, does not require large computing resources, and corresponds to the task posed in the study.

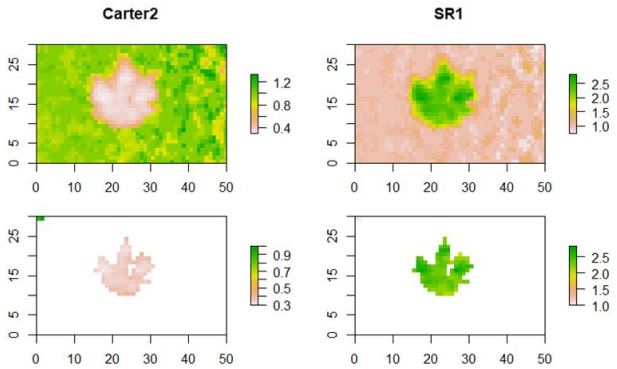

Figure 7. Carter2 and SR1 VIs values linked to specific spectra in the hyperspectral image before and after «cleaning».

In particular, it should be noted that in several works, attention is not paid to the analysis of the nature of the distribution of sets of VIs values. The choice of approach to mathematical data processing depends on the type of distribution; the distribution indirectly indicates the representativeness of the sample. Thus, a serious question about the representativeness of the sample arises with an asymmetric distribution. Therefore, sets of VI values were tested for normal distribution according to four criteria: Shapiro-Wilk, Pearson, Lilliefors, and Cramer-Mises. The results of testing the distribution of the spectrum sets of samples of all three tree species as of the survey date of August 26 in terms of VIs values are presented in supplementary Table 4. In most cases, the distribution of the spectra of a leaf blade in terms of VIs value does not follow a normal distribution. The largest number (approaching 50%) of populations distributed according to the normal law was noted for the indices CI2, ClAInt, Gitelson2, mSR2, NDVI2, OSAVI2, SR1, TCARI2/OSAVI2, TGI, Vogelmann, Vogelmann2. An analysis of the VIs distributions showed that the curve describing them is a bell-shaped shape and gradually approaches the abscissa axis along the edges. The dynamics of changes in the nature of the distribution of NDVI and PSSR of *A. campestre* from image to species on the HSI date of August 26 are presented in Table 1 and Figures 8 and 9. It should be noted that in this sequence, the general patterns of distribution (the direction of kurtosis and asymmetry) do not change. The resulting distributions have an average skewness index ($0.1 \leq |A_s| \leq 0.6$) and a large positive kurtosis coefficient ($E_x > 1$). The mode (M_o) and median (M_e) values are very close.

Table 1. Statistical characteristics of samples of NDVI and PSSR values for *A. campestre* in dynamics from one snapshot to all snapshots of species.

VI			NDVI				PSSR	
Object	snapshot	leaf	sample	species	snapshot	leaf	sample	species
M_e	0.606	0.611	0.605	0.602	7.143	6.974	6.444	6.571
M_o	0.601	0.606	0.603	0.600	7.786	6.938	6.972	6.741
E_x	3.156	3.205	3.063	2.969	2.273	2.562	2.623	2.924
A_s	−0.560	−0.599	−0.361	−0.341	−0.132	0.145	0.202	0.382

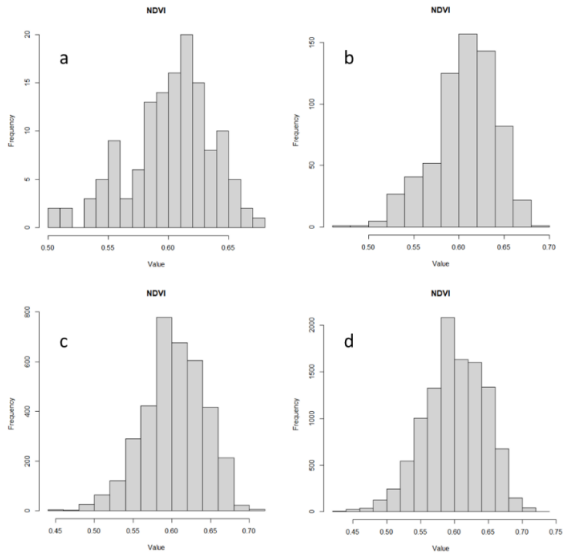

Figure 8. *A. campestre* NDVI magnitude distribution obtained from a set of spectra with PSSR values ranging from 5 to 10 in sequence from one snapshot to all snapshots of species. *a* – snapshot; *b* – leaf; *c* – sample; *d* – species.

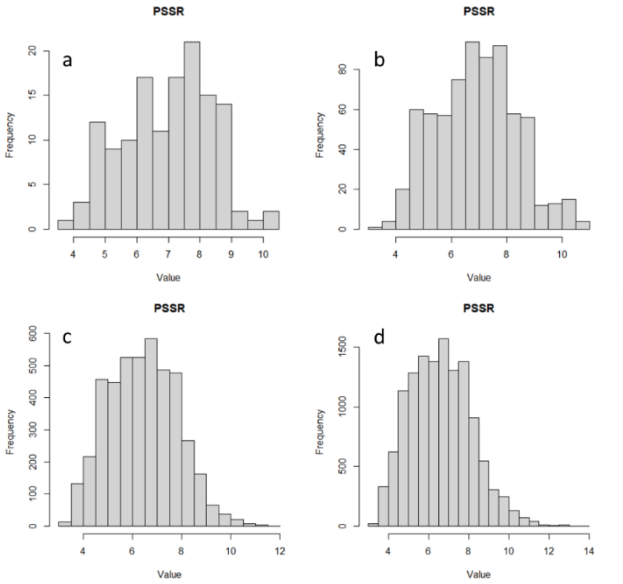

Figure 9. *A. campestre* PSSR distribution by magnitude obtained from a set of spectra with NDVI values ranging from 0.5 to 1.0 in sequence one snapshot to all snapshots of species. *a* – snapshot; *b* – leaf; *c* – sample; *d* – species.

Analysis of variance was used to determine the contribution of experimentally controlled factors («leaf», «sample», «species») to the VI value. The use of the parametric method for data analysis with the established nature of the distribution of index values is due to its closeness to the normal type, large sample size, coincidence of mode and median values. The results of a three-way analysis of variance for the NDVI value in the first period of the experiment (Aug 26) are shown in Table 2. All other VIs in supplementary Table 5.

Table 2. Results of a three-way ANOVA of the «species-sample-leaf» statistical complex for the NDVI value.

ANOVA	Df	Sum Sq	Mean Sq	F value	Pr(>F)
Species	2	7.040	3.520	2662.44	<2e−16*
Sample	6	4.872	0.812	614.23	<2e−16*
Leaf	54	4.106	0.076	57.52	<2e−16*
Intragroup variance	6002	7.935	0.001		

Note: * significance level < 0.001

VI satisfies the problem of species identification well if, according to the results of ANOVA Sum. Sq. factor «Species» is greater than the factor «Sample», Sum. Sq. factor «Sample» is greater than the factor «Leaf», Sum. Sq. factor «Species» is greater than the intra-group variance. It means that the value of the index depends more on species characteristics than on other factors. These VIs include Datt2", "Datt", "Maccioni", "CRI2", "SR6", "mSR2", "CARI", "REP_Li", "CRI4", "Carter4", "CI2", "DD ", "SR", "Vogelmann", "NDVI2", "OSAVI2", "MCARI", "GMI2". It should be noted that the value of almost all VIs is more dependent on the «Leaf» factor than on the «Sample» factor. Thus, we believe that we have a representative set of data formed per the task set – the identification of woody plant species based on hyperspectral survey data.

Our next step involved the use of principal component analysis (PCA)to establish the relationship between 80 VIs values and experimental species. The PCA results, depicted in Figure 10, Are particularly reassuring. They showed that the location of the species on the projection remains consistent over time, indicating the stability of the findings. Additionally, the dispersions of the first and second principal components, as shown in Table 3, do not exceed 0.70. This suggests that, the influence of subsequent components on the total variance is negligible, further bolstering the reliability of our results.

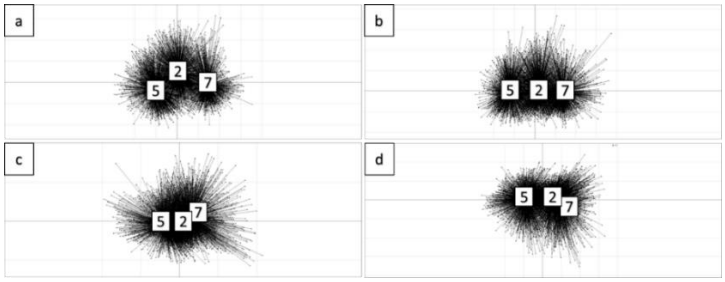

Figure 10. Projection of Vegetation Index Values *A. campestre* (2), *T. cordata* (5) and *U. pumila* (7). Sampling dates: Aug 26 (a), Sept 02 (b), Sept 09 (c), Sept 15 (d).

Table 3. The value of the variances attributable to the first and second principal components of the projection of 80 VIs values for *A. campestre*, *T. cordata*, *U. pumila* on different sampling dates.

Statistics	Aug 26		Sept 02		Sept 09		Sept 15	
	Comp.1	Comp. 2	Comp. 1	Comp. 2	Comp. 1	Comp. 2	Comp. 1	Comp. 2
Standard deviation	5.600	4.334	5.838	4.030	5.285	4.483	5.779	4.080
Proportion of Variance	0.392	0.234	0.426	0.203	0.349	0.251	0.417	0.208
Cumulative Proportion	0.392	0.627	0.426	0.629	0.349	0.600	0.417	0.625

Therefore, it was decided to divide the species into pairs. Determine the VIs that mainly contribute to the variance of the first principal component for each pair of species. Then combine all the established VIs into one group and try to separate all three types simultaneously by their values. Visualization of the projection of 80 VIs values for a pair of *A. campestre* and *U. pumila* shows a clear separation of these species (Figure 11).

In this case, the Proportion of Variance for the first and second principal components is only 0.616. In total, there are 10 significant components in accordance with the Kaiser criterion (the number of factors is equal to the number of components whose Proportion of Variance is greater than 0.01) (Table 4). It cannot be considered satisfactory for such experiments.

Based on factor loads (supplementary Table 6), the most informative VIs were selected – Carter2, CI2, CRI4, GMI2, mSR2, NDVI2, OSAVI2, and SR1. Table 5 shows the value of the values of these indices for *A. campestre* and *U. pumila*. In that case, it was possible to obtain the maximum range of variability along the axis of the first component, while minimizing it along the axis of the second component (Figure 12).

The value of the Proportion of Variance, which falls on the first principal component, is 0.979. The number of significant components in accordance with the Kaiser criterion was reduced to two. The reliability of the results confirms their repeatability in terms of sampling (supplementary Table 7).The factor loadings of the selected VIs on the first significant component became higher in Table 6.

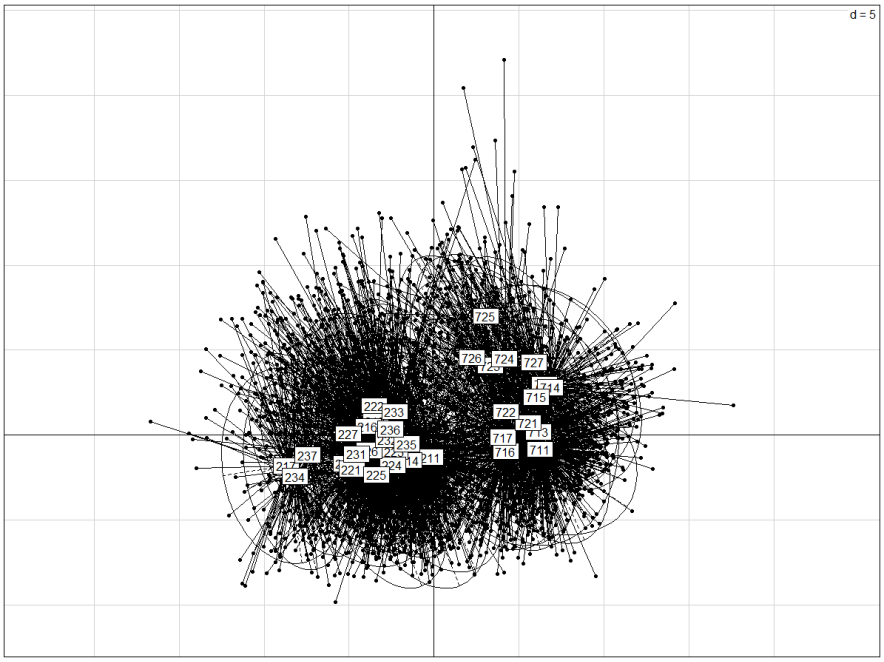

Figure 11. Projection of 80 VIs values of *A. campestre* and *U. pumila* (Aug 26). The first digit in the number indicates the species number (*A. campestre* – 2, *U. pumila* – 7), the second – the sample number, the third – the leaf number.

Table 4. The value of the variance of the main components of the projection of the values of vegetation indices for *A. campestre* and *U. pumila* (Aug 26).

Statistics / Component	1	2	3	4	5	6	7	8	9	10
Standard deviation	5.466	4.402	2.763	2.349	1.689	1.607	1.222	1.176	1.099	1.041
Proportion of Variance	0.374	0.242	0.095	0.069	0.036	0.032	0.019	0.017	0.015	0.014
Cumulative Proportion	0.374	0.616	0.711	0.780	0.816	0.848	0.867	0.884	0.899	0.913

Table 5. The value of the variance of the main components of the projection of the values of the Carter2, CI2, CRI4, GMI2, mSR2, NDVI2, OSAVI2, SR1 VIs values for *A. campestre* and *U. pumila* (Aug 26).

Statistics	Comp. 1	Comp. 2
Standard deviation	2.797	0.304
Proportion of Variance	0.978	0.011
Cumulative Proportion	0.978	0.990

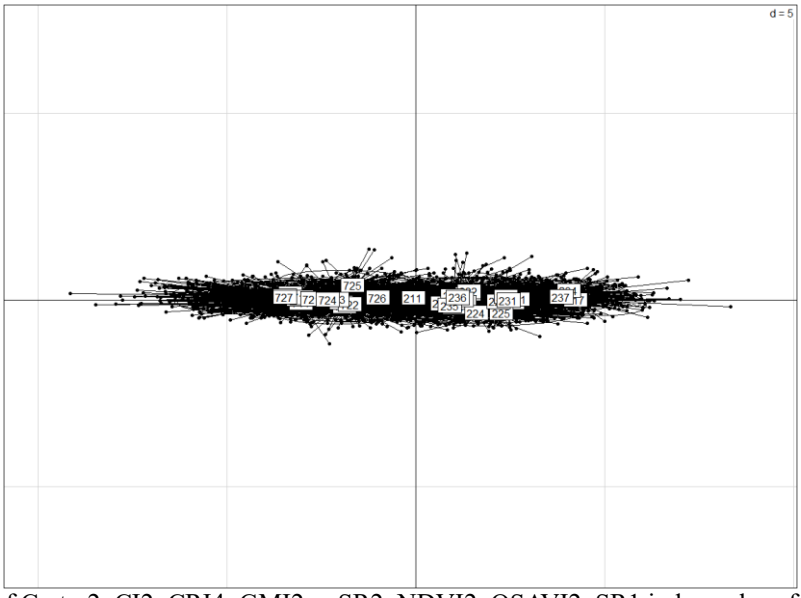

Figure 12. Projection of Carter2, CI2, CRI4, GMI2, mSR2, NDVI2, OSAVI2, SR1 index values for *A. campestre* and *U. pumila* (Aug 26). The first digit in the number indicates the species number (*A. campestre* – 2, *U. pumila* – 7), the second – the sample number, the third – the leaf number.

Table 6. Factor loadings obtained using the PCA method.

VI	Carter2	CI2	CRI4	GMI2	mSR2	NDVI2	OSAVI2	SR1
Comp.1	0.345	−0.355	0.354	−0.356	−0.354	−0.354	−0.354	−0.356

The visualization of the projection of 80 VIs values for the *T. cordata* and *U. pumila* pair onto the first two principal components (Figure 13), as well as for the *A. campestre* and *U. pumila* pair, shows a good separation of these species. However, in this case, the Cumulative Proportion of the first and second principal components is less than 0.70. Further, they acted following algorithm applied to the pair of *A. campestre* and *U. pumila.* For the *T. cordata* and *U. pumila* pair, the maximum factor load in the first component is Carter4, Datt2, mSR2, NDVI2, OSAVI2, and SR6. Figure 14 visualizes the projection of the Carter4, Datt2, mSR2, NDVI2, OSAVI2, and SR6 VI values for *T. cordata* and *U. pumila*.

The value of the Proportion of Variance, which falls on the first principal component, is 0.986. For the second component, it is already below 0.01 (Table 7). The reliability of the results confirms the repeatability of the results over the timing of sampling (supplementary Table 7).

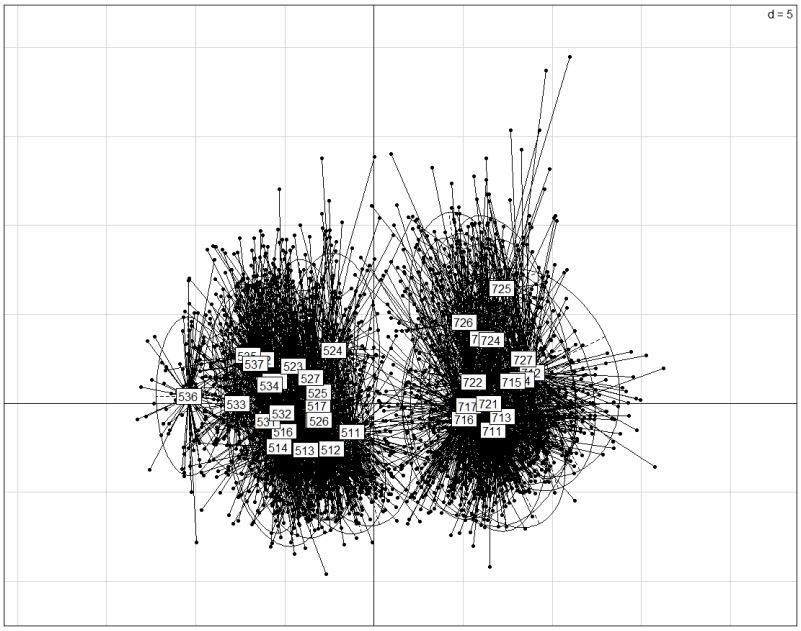

Figure 13. Projection of values of 80 vegetation indices of *T. cordata* and *U. pumila* (Aug 26). The first digit in the number indicates the species number (*T. cordata* – 5 and *U. pumila* – 7), the second – the sample number, the third – the leaf number.

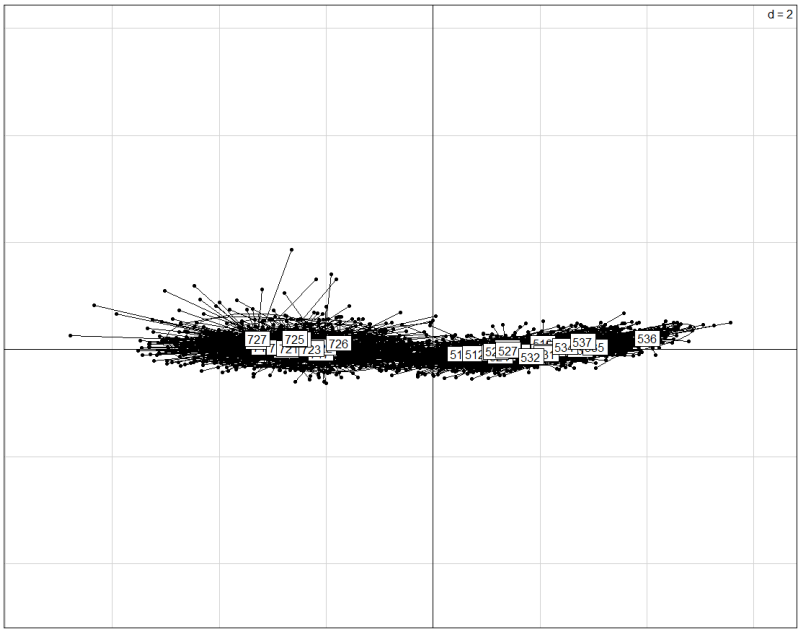

Figure 14. Projection of index values Carter4, Datt2, mSR2, NDVI2, OSAVI2, SR6 *T. cordata* (5) and *U. pumila* (7) (Aug 26). The first digit in the number indicates the species number (*T. cordata* – 5 and *U. pumila* – 7), the second – the sample number, the third – the leaf number.

Table 7. The value of the dispersion of the main components of the projection of the Carter4, Datt2, mSR2, NDVI2, OSAVI2, SR6 VI values for *A. campestre* and *U. pumila* (Aug 26).

Statistics	Comp. 1	Comp. 2
Standard deviation	2.432	0.215
Proportion of Variance	0.986	0.007
Cumulative Proportion	0.986	0.993

Visualization of the projection of the values of 80 VIs of *A. campestre* – *T. cordata* on the first two principal components (Figure 15), as well as for the previous ones, satisfactorily separates these species. However, in this case the Cumulative Proportion of the first and second principal components is less than 0.65. It has been established that for the *A. campestre* – *T. cordata* pair, Carter4, Datt, DD, Maccioni, MTCI, SR6 have the maximum factor load in the first component. The projection of their magnitude is shown in Figure 16. The Proportion of Variance value, which falls on the first principal component, is 0.935. The reliability of the results, as for the previous pairs of species, confirms the repeatability of the results over the timing of sampling (Table 8, supplementary Table 7).

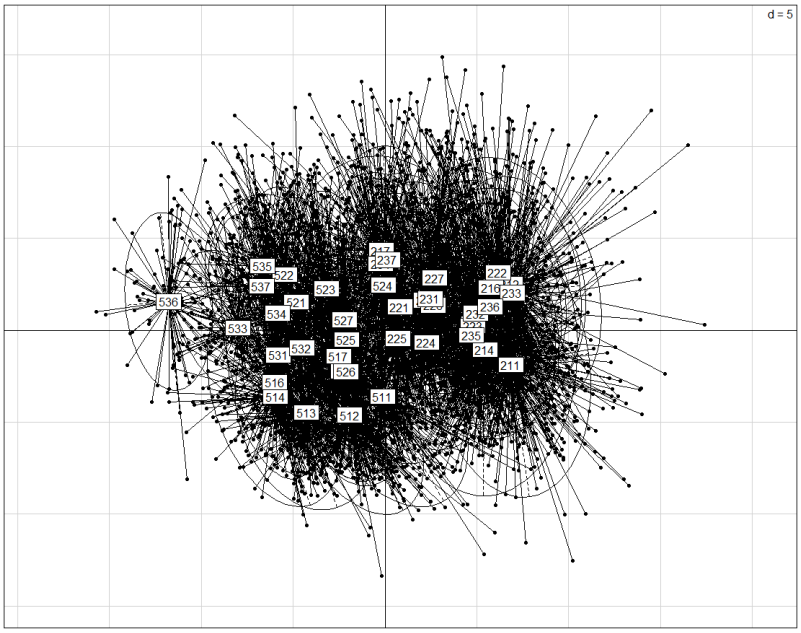

Figure 15. Projection of the values of 80 vegetation indices *A. campestre* – *T. cordata* (Aug 26). The first digit in the number indicates the species number (*T. cordata* – 5 and *A. campestre* – 2), the second – the sample number, the third – the leaf number.

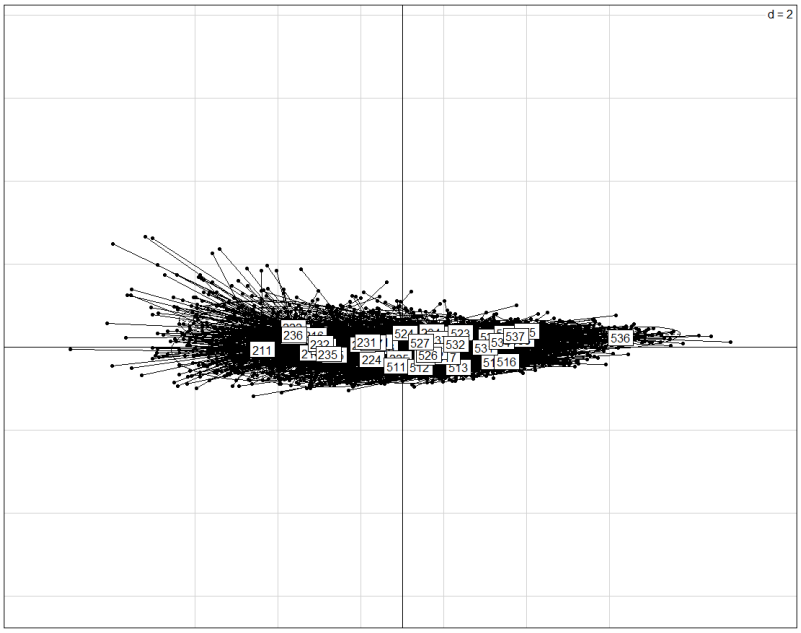

Figure 16. Projection of Carter4, Datt, DD, Maccioni, MTCI, SR6 *A. campestre* and *T. cordata* indices (Aug 26). The first digit in the number indicates the species number (*T. cordata* – 5 and *A. campestre* – 2), the second – the sample number, the third – the leaf number.

Table 8. The value of the variance of the principal components of the projection of the Carter4, Datt, DD, Maccioni, MTCI, SR6 CI values for *A. campestre* and *T. cordata* (Aug 26).

Statistics	Comp. 1	Comp. 2	Comp. 3
Standard deviation	2.368	0.430	0.314
Proportion of Variance	0.935	0.030	0.016
Cumulative Proportion	0.935	0.966	0.982

Further, all VIs selected for three pairs were combined into one group. These are Carter2, CI2, CRI4, GMI2, mSR2, NDVI2, OSAVI2, SR1, Carter4, Datt2, SR6, Datt, DD, Maccioni, and MTCI. Projections of the magnitude of these VIs belonging to *A. campestre, U. pumila* and *T. cordata* for four sampling periods are shown in Figure 17.

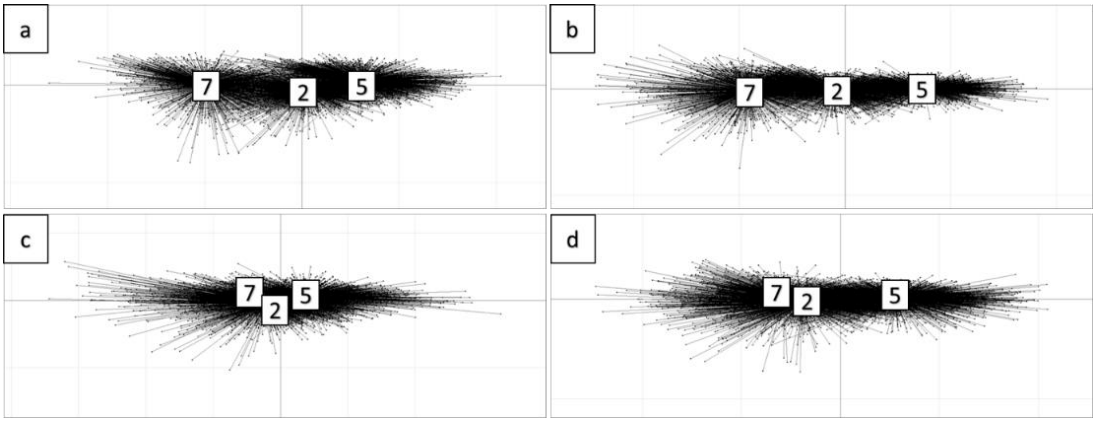

Figure 17. Projection of index values Carter2, CI2, CRI4, GMI2, mSR2, NDVI2, OSAVI2, SR1, Carter4, Datt2, SR6, Datt, DD, Maccioni, MTCI *A. campestre* (2), *T. cordata* (5), *U. pumila* (7).
Sampling dates: Aug 26 (a), Sept 02 (b), Sept 09 (c), Sept 15 (d).

The technique used made it possible not only to concentrate practically the entire dispersion in one plane, but also to stretch it as much as possible along the axis of the first principal component. All projections are characterized by a large Proportion of Variance for the first principal component (more than 0.90) and, accordingly, a small Proportion of Variance for the second principal component (Table 9). The Proportion of Variance values of the subsequent components are not significant. It should be especially noted that the arrangement of species along the axis of the main component remains constant in all four periods. Since the results obtained at different times of leaf sampling are independent, we can talk about their certain convergence. The factor load on the first significant component, although increased, remains low after selection of VI (Table 10).

Table 9. The value of the variance attributable to the first and second principal components of the projection of the values of the vegetation indices Carter2, CI2, CRI4, GMI2, mSR2, NDVI2, OSAVI2, SR1, Carter4, Datt2, SR6, Datt, DD, Maccioni, MTCI for *A. campestre*, *T. cordata*, *U. pumila* at different sampling dates.

Statistics / Component	Aug 26		Sept 02		Sept 09		Sept 15	
	1	2	1	2	1	2	1	2
Standard deviation	3.756	0.713	3.792	0.540	3.710	0.837	3.781	0.599
Proportion of Variance	0.941	0.033	0.959	0.019	0.917	0.046	0.953	0.023
Cumulative Proportion	0.941	0.974	0.959	0.978	0.917	0.964	0.953	0.977

Table 10. VI factor loads on the first component.

VI / Date of sampling	Aug 26	Sept 02	Sept 09	Sept 15
Carter2	0.249	0.251	0.243	0.250
CI2	−0.261	−0.260	−0.262	−0.260
CRI4	0.260	0.260	0.260	0.260
GMI2	−0.261	−0.260	−0.262	−0.260
mSR2	−0.264	−0.262	−0.266	−0.262
NDVI2	−0.264	−0.262	−0.266	−0.263
OSAVI2	−0.264	−0.262	−0.266	−0.263
SR1	−0.261	−0.260	−0.262	−0.260
Carter4	0.264	0.261	0.265	0.262
Datt2	−0.257	−0.258	−0.253	−0.254
SR6	−0.264	−0.262	−0.266	−0.262
Datt	−0.252	−0.255	−0.247	−0.252
DD	−0.253	−0.255	−0.253	−0.256
Maccioni	−0.251	−0.256	−0.252	−0.256
MTCI	−0.245	−0.248	−0.246	−0.251

None of the VIs is significantly distinguished by its value, therefore, when identifying tree species, it is necessary to use a group of VIs, the number of which is to be determined. We assume that it is possible to determine the VI most significant for identifying tree species only under the conditions of a strictly set laboratory experiment. It seems almost impossible to do this based on field HSI of crowns from the ground or air, individual shoots, and leaves, subject to the superposition of uncontrolled factors (illumination, distance to the object, the nature of the leaf mosaic of the crown, etc.). It is indicated by the data of the analysis of variance, according to which (even in the conditions of a laboratory experiment) the shares in the total variance of the factors «Sample» and «Leaf» are very significant. Intragroup variability is also of high importance.

Research showed that the PCA method is effective and sufficient to identify the group of VIs characterized by the largest dispersion in relation to tree species. Carrying it out in stages (by pairs of researched species) made it possible to identify a group of Vis whose value depends most on species characteristics. These are Carter2, CI2, CRI4, GMI2, mSR2, NDVI2, OSAVI2, SR1, Carter4, Datt2, SR6, Datt, DD, Maccioni, and MTC. This set of VIs will be used to identify tree species from crown images.

4. Conclusion

A technique has been developed to automatically select pure spectral profiles from hyperspectral images of plant objects. The selection is implemented by setting a double barrier, determined by the interval values of the PSSR and NDVI indices. The study has not only determined the main characteristics and assessed the representativeness of the sample datasets obtained from processing hyperspectral images of plant species but also found that the sample populations have a symmetrical distribution with high kurtosis based on their statistical characteristics. The aggregates are highly suitable for processing by both parametric and non-parametric methods, thereby providing implications for future research in this field. Principal component analysis, a crucial tool in our research, was used to identify the most informative VIs, including Carter2, CI2, CRI4, GMI2, mSR2, NDVI2, OSAVI2, SR1, Carter4, Datt2, SR6, Datt, DD, Maccioni and MTCI. These VIs not only allow the identification of woody species but also offer the possibility of repeating the effect over time, significant finding in our study. Currently, there is no clear answer to whether the unsatisfactory reproducibility of spectral remote sensing results in time and space is an insurmountable technological barrier or if it can be resolved through improved techniques and modeling processes. The answer to this question can be found by analyzing the results of laboratory experiments that use detailed time series of the spectral characteristics of various plant species throughout their growing season. Hyperspectral cameras are necessary equipment for such studies. Further research should be conducted to address this question.

Ethics Committee Approval: N/A.

Peer-review: Externally peer-reviewed.

Author Contributions: Concept: P.A.D., B.L.K; Design: P.A.D.; Supervision: A.A.D.; Resources: T.V.V.; Data Collection: P.A.D., A.A.D.; Analysis: P.A.D., B.L.K.; Literature Search: B.L.K.; Writing Manuscript: P.A.D., B.L.K., A.A.D.; Critical Review: P. A.D., B.L.K.

Conflict of Interest: The authors have no conflicts of interest to declare.

Financial Disclosure: The research was financially supported by the Ministry of Science and Higher Education of the Russian Federation (no. FENW-2023-0008).

Cite this paper as: Dmitriev, P.A., Kozlovsky, B.L., Dmitrieva, AA., Varduni, T. V. 2024. Potential of Geospatial Technologies in Mechanized Timber Harvesting Planning, *European Journal of Forest Engineering*, 10(1):54-66.

Acknowledgements
The research was performed with the equipment of Multiaccess Center 'Biotechnology, biomedicine and environmental monitoring' and Multiaccess Center 'High technologies' of Southern Federal University (Rostov-on-Don).

References

Aasen, H., Burkart, A., Bolten, A., Bareth, G. 2015. Generating 3D hyperspectral information with lightweight UAV snapshot cameras for vegetation monitoring: From camera calibration to quality assurance. *JPRS*, 108:245-259. https://doi.org/ 10.1016/ j.isprsjprs.2015.08.002

Aneta, M., Fassnacht, F.E., Stereńczak, K. 2020. Tree species identification within an extensive forest area with diverse management regimes using airborne hyperspectral data. *International Journal of Applied Earth Observation and Geoinformation*, 84: 101960, doi.org/10.1016/j.jag.2019.101960

Bareth, G., Aasen, H., Bendig, J., Gnyp, M.L., Bolten, A., Jung, A., Michels, R., Soukkamäki, J. 2015. Low-weight and UAV-based hyperspectral full-frame cameras for monitoring crops: Spectral comparison with portable spectroradiometer measurements. Photogramm. Fernerkundung, *Geoinf*. 69-79. https://doi.org/10.1127/pfg/2015/0256.

Cao, J., Leng, W., Liu, K., Liu, L., He, Z., Zhu, Y. 2018. Object-Based mangrove species classification using unmanned aerial vehicle hyperspectral images and digital surface models. *Remote Sens.,* 10:89. https://doi.org/10.3390/rs10010089.

Chen, C., Jing, L., Li, H., Tang, Y., Chen, F. 2023. Individual Tree Species Identification Based on a Combination of Deep Learning and Traditional Features. *Remote Sens.* 15: 2301

Dainelli, R., Toscano, P., Di Gennaro, S.F., Matese, A. 2021. Recent Advances in Unmanned Aerial Vehicles Forest Remote Sensing - a Systematic Review. Part II: Research Applications. *Forests*, 12(4):397. https://doi.org/10.3390/f12040397.

Dmitriev, P.A., Kozlovsky, B.L., Kupriushkin, D.P., Lysenko, V.S., Rajput, V.D. et al. 2022a. Identification of species of the genus Acer L. using vegetation indices calculated from the hyperspectral images of leaves. *Remote Sensing Applications: Society and Environment*, 100679. https://doi.org/10.1016/j.rsase.2021.100679.

Dmitriev, P.A., Kozlovsky, B.L., Kupriushkin, D.P., Dmitrieva, A.A., Rajput, V.D. et al. 2022b. Assessment of Invasive and Weed Species by Hyperspectral Imagery in Agrocenoses Ecosystem. *Remote Sens*., 14:2442. https://doi.org/10.3390/ rs14102442.

Egli, S., Höpke, M. 2020. CNN-Based Tree Species Classification Using High Resolution RGB Image Data from Automated UAV Observations. *Remote Sens.,* 12:2-17. https://doi.org/10.3390/rs12233892.

Fassnacht, F.R., White, J.C., Wulder, M.A., Næsset, E. 2024. Remote sensing in forestry: current challenges, considerations and directions, *Forestry: An International Journal of Forest Research,* 97(1): 11–37. https://doi.org/10.1093/forestry/ cpad024

Grabska, E., Frantz, D. and Ostapowicz, K. 2020 Evaluation of machine learning algorithms for forest stand species mapping using Sentinel-2 imagery and environmental data in the polish Carpathians. *Remote Sens. Environ.* 251, 112103. https://doi.org/10.1016/ j.rse.2020.112103.

Hermosilla, T., Bastyr, A., Coops, N.C., White, J.C., Wulder, M.A. 2022 Mapping the presence and distribution of tree species in Canada's forested ecosystems. *Remote Sens. Environ.* 282, 113276. https://doi.org/10.1016/j.rse.2022.113276.

Heupel, K., Spengler, D., Itzerott, S.A. 2018. Progressive Crop-Type Classification Using Multitemporal Remote Sensing Data and Phenological Information. *PFG*, 86:53-69. https://doi.org/10.1007/s41064-018-0050-7.

Zhang, J., Zhang, Y., Zhou, T., Sun, Y., Yang, Z., Zheng, S. 2023. Research on the identification of land types and tree species in the Engebei ecological demonstration area based on GF-1 remote sensing, Ecological Informatics, 77(2023): 102242, ISSN 1574-9541, https://doi.org/10.1016/j.ecoinf.2023.102242

Onishi, M., Ise, T. 2021. Explainable identification and mapping of trees using UAV RGB image and deep learning. *Scientific Reports.* 11(1):1-15. https://doi.org/10.1038/s41598-020-79653-9.

Panov, V.D., Lurie, P.M., Larionov, Y.A. 2006. The Climate of the Rostov Region: Yesterday, Today, Tomorrow. Donskoy Publishing House: Rostov-on-Don, Russia, p. 488.

R Core Team, R: A language and environment for statistical computing. R Foundation for Statistical

Computing, Vienna, Austria. https://www.r-project.org/ (date of circulation: December 01, 2023).

Saeed, S., Latif, M.A., Rajput, M.A. 2021. Fuzzy-Based Multi-Crop Classification Using High Resolution UAV Imagery. *Quaid-E-Awam University Research Journal of Engineering, Science & Technology, Nawabshah,* 19(1):1-8. https://doi.org/10.52584/QRJ.1901.01.

Sothe, C., De Almeida, C.M., Schimalski, M.B., La Rosa, L.E.C., Castro et al. 2020. Comparative performance of convolutional neural network, weighted and conventional support vector machine and random forest for classifying tree species using hyperspectral and photogrammetric data. *GIScience Remote Sens.,* 57:369-394. https://doi.org/10.1080/15481603.2020.1712102.

van der Werff, H., Ettema, J., Sampatirao, A., Hewson, R. 2022. How Weather Affects over Time the Repeatability of Spectral Indices Used for Geological Remote Sensing. *Remote Sens.* 14: 6303. https://doi.org/10.3390/rs14246303

Vannoppen, A., Gobin, A., Kotova, L., Buntemeyer, L., Remedio, A.R. et al. 2020. Wheat yield estimation from ndvi and regional climate models in Latvia. *Remote Sensing.,* 12(14):2206. https://doi.org/10.3390/rs12142206.

Zhong, H., Lin, W., Liu, H., Ma, N., Liu, K., Cao, R., Wang, T., Ren, Z. 2022. Identification of tree species based on the fusion of UAV hyperspectral image and LiDAR data in a coniferous and broad-leaved mixed forest in Northeast China. *Front. Plant Sci.* 13:964769. doi: 10.3389/fpls.2022.964769.